Energy Conservation as a Principle Underlying Mobilizable Strength Design for Deep Excavations

S. Y. Lam[1] and M. D. Bolton[2]

Abstract: Finite-element analyses (FEA) and case histories of deep excavations in soft clay are used to validate a decision-making tool based on an extended mobilizable strength design (MSD) method that permits the designer an extremely simple method of predicting ground displacements during an undrained excavation. This newly extended MSD approach accommodates a number of issues that are important in underground construction between in situ walls, including alternative base heave mechanisms suitable either for wide excavations in relatively shallow soft clay strata or narrow excavations in relatively deep soft strata, the influence of support system stiffness in relation to the sequence of propping of the wall, and the capability of dealing with stratified ground. In addition, a simplified MSD framework is proposed for analyzing a database of 110 deep excavation case histories worldwide. The approach examines the governing factors controlling deformation in deep excavations and offers simple guidelines for designing support structures for deep excavations. These developments should make it possible for a design engineer to make informed decisions on the relationship between prop spacing and ground movements or the influence of wall stiffness and on the need for and influence of a jet-grouted base slab, for example, prior to conducting project-specific FEA. **DOI: 10.1061/(ASCE)GT.1943-5606.0000510.**

CE Database subject headings: Energy efficiency; Case studies; History; Excavation; Stiffness.

Author keywords: Mobilizable strength design; Case histories; Deep excavation; Soil stiffness.

Introduction

The mobilizable strength design (MSD) method has its origins in attempts to use plastic deformation mechanisms to predict ground displacements around retaining walls: (Milligan and Bransby 1976; Bolton and Powrie 1987; Bolton et al. 1989, 1990a, b). Separate but broadly consistent mechanisms were used to represent the states of equilibrium of soil bodies adjacent to a wall and their possible states of deformation. The demands of equilibrium were first applied to deduce a mobilized soil strength. Raw shear stress-strain data from soil tests on representative undisturbed samples could then be used directly to link stresses and strains under working conditions and thereby to deduce soil strains and wall movements.

The fully developed MSD approach, on the other hand, requires the engineer only to imagine the kinematics (i.e., the pattern of displacements) of the soil caused by the proposed actions. This deformation mechanism will immediately imply a compatibility relationship between the average strain mobilized in the soil and the boundary displacements. It is then necessary to provide representative stress-strain data for the soils participating in the mechanism. Just as with an upper bound plastic analysis of collapse, the requirement for a separate equation of equilibrium can then be replaced by the consideration of work and energy in the selected mechanism. In the case of MSD, however, this energy equation is related to working stresses and the prediction of deformations in service.

The MSD approach has been successfully implemented for shallow foundations (Osman and Bolton 2005), cantilever retaining walls (Osman and Bolton 2004), tunneling-induced ground displacements (Osman et al. 2006) and also the sequential construction of braced excavations that induce wall displacements and ground deformations (Osman and Bolton 2006). Recent work by Klar and Osman (2008) further clarified the approach to MSD through the principle of energy conservation. This is further extended to deep excavations in the current work, following Bolton et al. (2009), in which changes of gravitational potential energy and the strain energy of the supporting structure are included in the formulation for the first time.

Current Design Approach for Braced Excavations

Plastic Failure Mechanisms

Limit equilibrium methods are routinely used in stability calculations for soft clay that is overidealized as rigid-plastic. Slip surfaces are selected as the assumed focus of all plastic deformations. Failure mechanisms should be kinematically admissible, meaning that neither unwanted gaps nor overlaps should be produced. Furthermore, in the case of undrained shearing of clays, a constant-volume condition should be respected at every point. A consequence is that undrained plane-strain failure mechanisms must comprise only slip planes and slip circles. The soil on such failure surfaces is taken to mobilize its undrained shear strength divided by a safety factor to maintain the mechanism in limiting equilibrium under the action of gravity and any other applied loads. If preferred, the same calculation can be set up as a balance of work done and energy dissipated as the result of an arbitrary displacement of the mechanism, which then cancels out. Calculated in this way, the safety factor literally offers an estimate of the factor by which the strength of the soil

[1]Ph.D. Student, Dept. of Engineering, Univ. of Cambridge, United Kingdom (corresponding author). E-mail: syl33@eng.cam.ac.uk

[2]Professor, Dept. of Engineering, Univ. of Cambridge, United Kingdom. E-mail: mdb@eng.cam.ac.uk

Note. This manuscript was submitted on August 24, 2009; approved on January 14, 2011; published online on January 17, 2011. Discussion period open until April 1, 2012; separate discussions must be submitted for individual papers. This paper is part of the ***Journal of Geotechnical and Geoenvironmental Engineering***, Vol. 137, No. 11, November 1, 2011. ©ASCE, ISSN 1090-0241/2011/11-1062–1074/$25.00.

would have to drop before the soil construction would collapse. Such estimates will err on the high side if the assumed mechanism departs from reality in any given case.

In the case of base heave in braced excavations, plastic solutions were derived from slip-line fields based on the method of characteristics. Such solutions comprise both slip surfaces, as before, and plastic fans, which distribute plastic strains over a finite zone in the shape of a sector of a circle. Notwithstanding these zones of distributed strain, the additional presence of slip surfaces still restricts the application of these solutions to the prediction of failure. Furthermore, no such solution can be regarded automatically as an accurate predictor of failure, notwithstanding their apparent sophistication. Their use in practice can only be justified following back-analysis of actual failures, whether in the field or the laboratory.

Fig. 1 shows two typical failure mechanisms, as suggested by Terzaghi (1943) and Bjerrum and Eide (1956). They have each been widely used for the design of multipropped excavations. Terzaghi (1943) suggested a mechanism consisting of a soil column outside the excavation, which creates a bearing-capacity failure. The failure is resisted by the weight of a corresponding soil column inside the excavation and also by adhesion acting along the vertical edges of the mechanism. Bjerrum and Eide (1956) assumed that the base of the excavation could be treated as a negatively loaded perfectly smooth footing. The bearing-capacity factors proposed by Skempton (1951) are used directly in the stability calculations and are taken as stability numbers, $N = \gamma H/c_u$. Eide et al. (1972) modified this approach to account for the increase in basal stability owing to mobilized shear strength along the embedded length of the rigid wall.

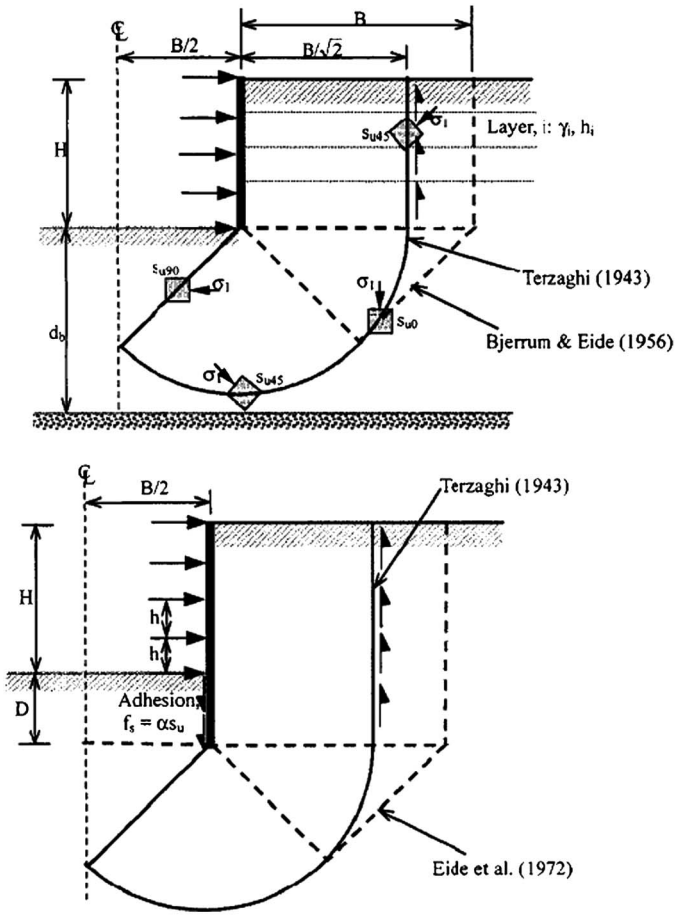

Fig. 1. Conventional basal stability mechanism and notation (after Ukritchon et al. 2003 ASCE): (a) without wall embedment (principal stress directions after Clough and Hansen 1981); (b) with wall embedment

O'Rourke (1993) further modified the basal stability calculations of Bjerrum and Eide (1956) to include flexure of the wall below the excavation level. It was assumed that the embedded depth of the wall does not change the geometry of the basal failure mechanism. However, an increase in stability was anticipated as a result of the plastic work done on the wall. This gave stability numbers that were functions of the yield moment and of the assumed boundary conditions at the base of the wall.

Ukritchon et al. (2003) used numerical limit analysis to calculate the stability of braced excavations. Upper and lower bound formulations were presented on the basis of Sloan and Kleeman (1995) and Sloan (1988), respectively. The technique calculates upper-bound and lower-bound estimates of collapse loads numerically by linear programming, whereas spatial discretization and interpolation of the field variables are calculated using the finite-element method. No failure mechanism needs to be assumed, and failure both of the soil and the wall are taken care of. However, both soil and wall are again assumed to be rigid perfectly plastic, so the failure mechanism includes a plastic hinge at the lowest level of support.

All these collapse limit analyses provide useful guidance on the possible geometry of plastic deformation mechanisms for service conditions. But the key requirement for MSD mechanisms is that displacement discontinuities (slip surfaces) must be avoided entirely. In that way, small but finite ground displacements are associated at every internal point with small but finite strains.

Wall Deformations

Clough et al. (1989) used field case records of braced excavations to plot the ratio of maximum wall movement to excavation depth (w_{max}/H) as a function of the support-system stiffness. Mana and Clough (1981) went on to plot a chart of w_{max}/H against the factor of safety against base heave as defined by Terzaghi (1943), ignoring the influence of the wall. They showed a very strong increase in wall bulging as the factor of safety of the soil dropped to unity or below. Although indicative guidelines were sketched on the chart, the scatter of the field data was rather wide. The current work intends to retain the simplicity inherent in such design charts while reducing scatter by better characterizing and analyzing deformation mechanisms.

At each stage of excavation in soft clay, the incremental displacement profile of the wall below the lowest prop will be assumed to be a cosine function, as described by O'Rourke (1993) and sketched in Fig. 2:

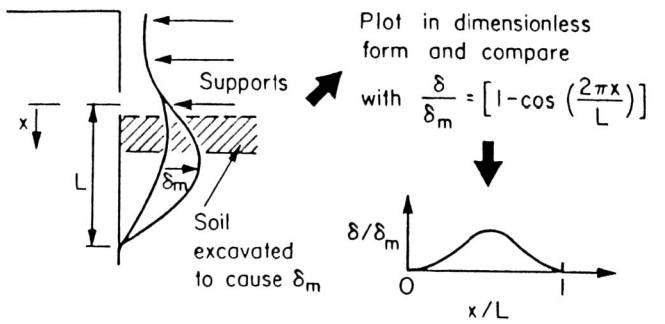

Fig. 2. Incremental displacements in braced excavation (after O'Rourke 1993)

$$\delta w = \frac{\delta w_{\max}}{2}\left[1 - \cos\left(\frac{2\pi y}{\lambda}\right)\right] \quad (1)$$

Here, δw = incremental wall displacement at any distance y below the lowest support; $\delta w_{\max}$ = its maximum value; and λ = wavelength of the deformation, defined by O'Rourke (1993) as the vertical distance from the lowest support to the level at which the wall is effectively fixed in a stiff underlying layer. Osman and Bolton (2006) noted that wavelength λ should therefore depend on the degree of wall base fixity. They expressed this in terms of the length s of the wall projecting below the lowest level of current support, by using a parameter α:

$$\lambda = \alpha s \quad (2)$$

For walls embedded into a stiff layer beneath soft clay such that the wall base is fully fixed in position and direction, α was set to 1. For walls embedded in deep soft clay, the maximum wall displacement occurs at the tip of the wall so the wavelength was taken as twice the projecting wall length ($\alpha = 2$). Intermediate cases were described as restrained-end walls ($1 < \alpha < 2$). It was recognized that this simple prescription could not accurately represent the actual soil–structure interaction, but it was also shown that MSD predictions made on the basis of it were nevertheless fairly good.

However, these kinematic conditions apply only to very wide excavations. When a narrow excavation is considered, the wavelength may be limited by the width of the excavation. This is considered next, together with other extensions and improvements to MSD for braced excavations.

Application of MSD for Deep Excavations

Osman and Bolton (2006) showed that for an in situ wall supporting an undrained deep excavation in soft clay, the total deformation can be approximated as the sum of the cantilever movement prior to propping and the subsequent bulging movement that accretes incrementally with every step in the sequence of propping and excavation.

A method for estimating the cantilever movement had been suggested earlier in Osman and Bolton (2004). It begins by considering the lateral earth pressure distribution for a smooth, rigid, cantilever wall rotating about a point some way above its toe in undrained conditions. A simple mobilized strength ratio is introduced to characterize the average degree of mobilization of undrained shear strength throughout the soil. By using horizontal force and moment equilibrium equations, the two unknowns (the position of the pivot point and the mobilized strength ratio) are obtained. Then a mobilized strain value is read off from the shear stress-strain curve of a soil element appropriate to the representative depth of the mechanism at the middepth of the wall. Simple kinematics for a cantilever wall rotating about its base suggests that the shear strain mobilized in the adjacent soil is double the angle of wall rotation. Accordingly, for the initial cantilever phase, the wall rotation is estimated as one-half of the shear strain required to induce the degree of mobilization of shear strength necessary to hold the wall in equilibrium. Osman and Bolton (2004) used finite-element analysis (FEA) to show that correction factors up to about 2.0 could be applied to these MSD estimates of the wall crest displacement, depending on a variety of nondimensional groups of parameters ignored in the simple MSD theory, such as wall flexibility and initial earth pressure coefficient prior to excavation.

A typical increment of bulging, on the other hand, was calculated in Osman and Bolton (2006) by considering an admissible plastic mechanism for base heave. In this case, the mobilized shear strength was deduced from the kinematically admissible mechanism itself, by using virtual work principles. The energy dissipated by shearing was said to balance the virtual loss of potential energy caused by the simultaneous formation of a subsidence trough on the retained soil surface and a matching volume of heave inside the excavation. The mobilized strength ratio could then be calculated, and the mobilized shear strain read off from the stress-strain curve of a representative element, as before. The wall deformation increment was then estimated by using the relationship between the boundary displacements and the average mobilized shear strain, in accordance with the original bulging mechanism.

The MSD solutions of Osman and Bolton (2006) compared quite well with some numerical simulations with the realistic nonlinear MIT-E3 model and various field case studies. However, these early solutions are capable of improvement in the following three ways, which will contribute to their applicability in engineering practice:

- The original mechanism assumed a relatively wide excavation, whereas cut-and-cover tunnel and subway constructions are likely to be much deeper than their width. The MSD mechanism therefore needs to be adapted for the case in which the plastic deformation fields for the side walls interfere with each other beneath the excavation.
- The structural strain energy of the support system can be incorporated. This could be significant when the wall is stiff and the soil is weak and especially so when measures are taken to limit base heave in the excavation, such as by base grouting between the supporting walls. In this case, the reduction of lateral earth pressure caused by ground deformation may be relatively small, and it is principally the stiffness of the structural system itself that limits external ground displacements.
- Progressively incorporating elastic strain energy requires the calculation procedure to be fully incremental, whereas Osman and Bolton (2006) used total energy flows to calculate the results of each stage of excavation separately. A fully incremental solution, admitting ground layering, will permit the accumulation of different mobilized shear strengths and shear strains at different depths in the ground, thereby improving accuracy.

This paper aims to introduce an enhanced MSD solution that includes these three features. This is then compared with an existing FEA study and with some case histories of braced excavation.

Geostructural Mechanisms and Extended MSD Method

Osman and Bolton (2006) proposed an incremental plastic deformation mechanism conforming to Eq. (1) for a wide multipropped excavation in clay. In this mechanism, the wall is assumed to be fixed incrementally in position and direction at the lowest prop, implying that the wall has sufficient strength to avoid the formation of a plastic hinge. The wall and soil are deforming compatibly, and the soil deformation also follows the cosine function of Eq. (1). The dimensions of this mechanism depend on the wavelength λ.

Fig. 3(a) shows the complete displacement field for the mechanism proposed by Osman and Bolton (2006). The solution includes four zones of distributed shear, which consist of a column of soil adjoining the excavation above the level of the lowest prop, a circular fan zone centered at the lowest prop, another circular fan zone with its apex at the junction of the wall and the excavation surface, and a 45° isosceles wedge below the excavation surface. The soil shears compatibly and continuously with no relative sliding at the boundaries of each zone. The dotted lines with arrows show the

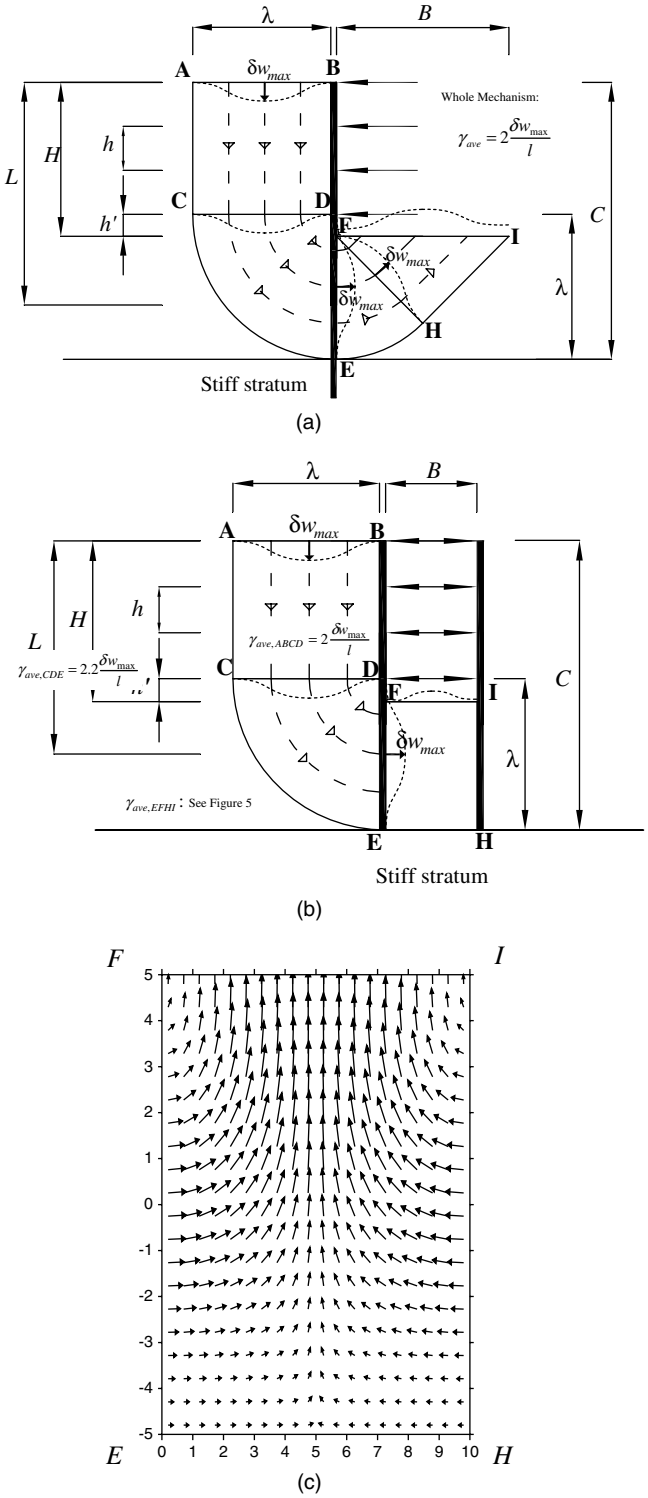

Fig. 3. Incremental displacement fields: (a) incremental displacement field for wide excavation; (b) incremental displacement field for narrow excavation; (c) incremental displacement field for narrow excavation for zone EFHI

direction of the flow. Along each of these lines, the displacement is constant and is given by the cosine function of Eq. (1). It is assumed that the zone outside the deformation zones is rigid. This mechanism of shearing at constant density is simple, but it only applies to wide excavations. In the case of a narrow excavation, the width of the triangular wedge could be bigger than the actual width of the excavation. In view of this, a new mechanism for narrow excavations is proposed in Fig. 3(b). The mechanism in the passive zone (zone EFHI) is replaced. The new mechanism [as shown in Fig. 3(c)] also meets the condition for undrained shearing, which means that the volumetric strain remains zero throughout the zone.

The original solution of Osman and Bolton (2006) assumed that soils were homogenous. The average shear strain increment in each zone was calculated by taking the derivative of the prescribed displacement equation. Then the undrained shear strength ($c_{u,\mathrm{mob}}$), mobilized at any location for any excavation height, was expressed using a single mobilization ratio $\beta = c_{u,\mathrm{mob}}/c_u$ to factor the strength profile. With the use of the virtual work principle, the plastic work done by shearing of the soil was equated to the virtual change of gravitational potential energy of the soil. A β factor was then found so that a corresponding mobilized shear strain could be read off from the chosen stress-strain curve. The incremental displacement was then calculated by the correlation between the average shear strain increment and the incremental wall displacement.

This approach offered a straightforward way to estimate the bulging displacement of the retaining wall. However, the approach requires refinement to include additional features that are significant in deep excavations. First, the approach did not consider the elastic strain energy stored in the support system. Second, it is common to find a nonuniform soil stratum with undrained shear strength that varies irregularly with depth. Furthermore, the geometry of the deformation mechanism changes as the construction proceeds, so the representation of mobilization of shear strength through the whole depth, by using a single mobilization ratio, is only a rough approximation. In reality, there will be differences in mobilization of shear strength at different depths for calculating incremental soil displacement.

Last, the original mechanism of Osman and Bolton (2006), shown in Fig. 3(a), only applied to wide excavations, which are defined with respect to Fig. 3(a) as indicating that the pair of retaining walls does not encroach so close as to cause their passive triangular zones FIH to overlap. Because the radius of the shear fan FHE is (λ-h'), in which h' = depth of excavation below the lowest prop, the wide excavation is defined by the condition $B \geq 2\sqrt{2}(\lambda\text{-}h')$. Conversely, the new mechanism, shown in Fig. 3(b), should be employed for narrow excavations defined by $B \leq 2\sqrt{2}(\lambda\text{-}h')$, for which the displacement field is given in Fig. 3(c).

Deformation Pattern in Different Zones

From Fig. 3, the soil is assumed to flow parallel to the wall at the retained side above the level of the lowest support (zone ABDC), and the incremental displacement at any distance x from the wall is given by the cosine function of Eq. (1), replacing y with x.

By taking the origin as the top of the wall, the deformation pattern of retained soil ABDC is given in rectangular coordinates as follows:

$$\delta w_y = -\frac{\delta w_{\max}}{2}\left[1 - \cos\left(\frac{2\pi x}{\lambda}\right)\right] \tag{3}$$

$$\delta w_x = 0 \tag{4}$$

In fan zone CDE, by taking the apex of the fan zone as the origin:

$$\delta w_y = \frac{\delta w_{\max}}{2}\left[1 - \cos\left(\frac{2\pi\sqrt{x^2+y^2}}{\lambda}\right)\right]\left(\frac{-x}{\sqrt{x^2+y^2}}\right) \tag{5}$$

$$\delta w_x = \frac{\delta w_{\max}}{2}\left[1-\cos\left(\frac{2\pi\sqrt{x^2+y^2}}{\lambda}\right)\right]\left(\frac{y}{\sqrt{x^2+y^2}}\right) \quad (6)$$

For fan zone EFH in a wide excavation, as indicated in Fig. 3(a), by taking the junction of the wall and the current excavation level as the origin:

$$\delta w_y = \frac{\delta w_{\max}}{2}\left[1-\cos\left(\frac{2\pi[h+\sqrt{x^2+y^2}]}{\lambda}\right)\right]\left(\frac{x}{\sqrt{x^2+y^2}}\right) \quad (7)$$

$$\delta w_x = \frac{\delta w_{\max}}{2}\left[1-\cos\left(\frac{2\pi[h+\sqrt{x^2+y^2}]}{\lambda}\right)\right]\left(\frac{y}{\sqrt{x^2+y^2}}\right) \quad (8)$$

For the triangular zone FHI in a wide excavation, again taking the junction of the excavation and the wall as the origin:

$$\delta w_y = \delta w_x = \frac{\sqrt{2}\delta w_{\max}}{4}\left[1-\cos\left(\frac{2\pi[h+\frac{\sqrt{2}}{2}(x-y)]}{\lambda}\right)\right] \quad (9)$$

For a narrow excavation, as shown in Fig. 3(b), a rectangular zone EFHI of two-dimensional (2D) shearing is now proposed. The origin is taken as the midpoint of FE, midwavelength in the excavation, at the wall:

$$\delta w_y = \frac{\lambda\delta w_{\max}}{4B}\left[\pi+\frac{2\pi y}{\lambda}+\sin\left(\frac{2\pi y}{\lambda}\right)\right]\left[\sin\left(\frac{\pi x}{B}\right)\right] \quad (10)$$

$$\delta w_x = \frac{\delta w_{\max}}{2}\left[1+\cos\left(\frac{2\pi y}{\lambda}\right)\right]\left[\cos\left(\frac{\pi x}{B}\right)\right] \quad (11)$$

In order to get more accurate solutions, it is supposed that the soil stratum is divided into n layers of uniform thickness (Fig. 4). The average shear strain $\delta\gamma(m,n)$ is calculated for the n layers in m excavation stages. The incremental engineering shear strain in each layer is calculated as follows:

$$\delta\gamma(m,n) = \frac{\int\left[\sqrt{(\frac{\partial w_x}{\partial y}+\frac{\partial w_y}{\partial x})^2-4\frac{\partial w_x}{\partial x}\frac{\partial w_y}{\partial y}}\right]d\mathrm{Vol}}{\int d\mathrm{Vol}} \quad (12)$$

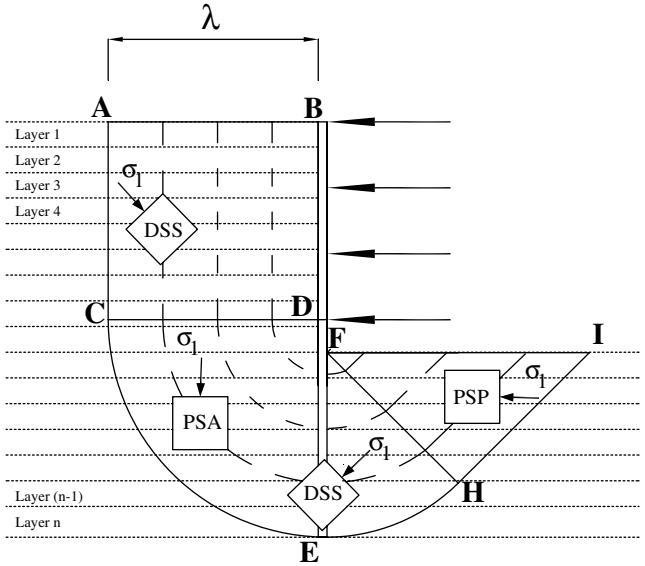

Fig. 4. Mobilizable shear strength profile of an excavation stage in a layered soil

In order to get a better idea of the deformation mechanism, the relationship between the maximum incremental wall displacement and the average shear strain mobilized in each zone of deformation should be obtained. On the active side of the excavation, the spatial scale is fixed by the wavelength of deformation λ, and all strain components are proportional to $\delta w_{\max}/\lambda$. The average engineering shear strain increment (γ_{mob}) mobilized in the deformed soil can be calculated from the spatial average of the shear strain increments in the whole volume of the deformation zone. For a wide excavation, as in Fig. 3(a), the average shear strain is equal to $2\delta w_{\max}/\lambda$. For a narrow excavation, the average shear strain (γ_{ave}) of active zone ABCD and fan zone CDE is $2\delta w_{\max}/\lambda$ and $2.23\delta w_{\max}/\lambda$, respectively, whereas γ_{ave} in the passive zone EFHI depends both on the wavelength λ of the deformation and the width B of the excavation. The relationship between the normalized average shear strain in EFHI and the excavation geometry (i.e., λ/B ratio) is shown in Fig. 5. Different excavation geometries are considered and indicated as black icons. The corresponding correlations are as follows:

$$\frac{\gamma_{\mathrm{ave}}}{2w_{\max}/B} = 0.38\left(\frac{2\lambda}{B}\right)+0.61 \quad \text{for } \frac{\lambda}{B}\geq 1 \quad (13)$$

$$\frac{\gamma_{\mathrm{ave}}}{2w_{\max}/B} = 0.98\left(\frac{2\lambda}{B}\right)^2-3.16\left(\frac{2\lambda}{B}\right)+3.83 \quad \text{for } \frac{\lambda}{B}\leq 1 \quad (14)$$

If an excavation has a width B that is slightly larger or smaller than $2\sqrt{2}(\alpha s-h')$, the two mechanisms should ideally produce identical wall displacements. Since the average shear strain inside the passive zone for the wide mechanism is $\gamma_{\mathrm{ave}}=2.23\delta w_{\max}/\lambda$ at the transition, and that of the narrow excavation is $\gamma_{\mathrm{ave}}=2.25\delta w_{\max}/\lambda$, this condition is satisfied sufficiently well.

Apart from the first excavation stage, all subsequent deformation mechanisms must partially overlay the previous ones (Fig. 6). Because of the nonlinearity of soil, it is important to calculate the accumulated mobilized shear strain in each particular layer of soil to correctly deduce the mobilized shear strength of that layer. This is done by an area-average method described as follows:

$$\gamma(m,n) = \frac{d\gamma(m,n)\times A(m,n)+\gamma(m-1,n)\times A(m-1,n)}{A(m,n)} \quad (15)$$

in which $\gamma(m,n)$ = total shear strain of the nth layer in the mth excavation stage, and $A(m,n)$ = area of deformation in the nth layer in the mth excavation stage.

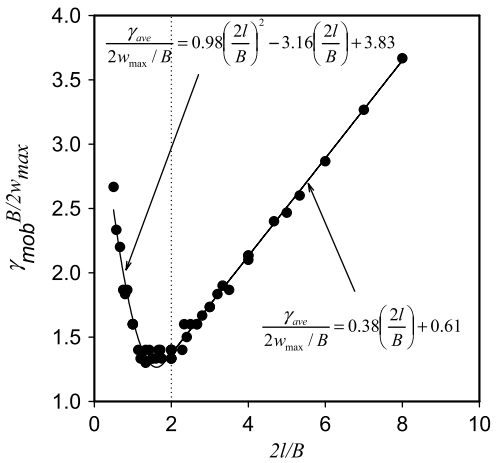

Fig. 5. Correlation between normalized average shear strain and excavation geometry for a narrow excavation

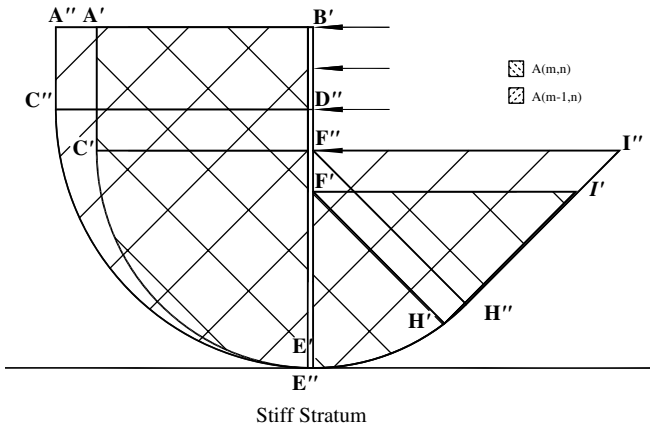

Fig. 6. Overlapping of deformation field

With the help of some suitable stress-strain relation for the soil (discussed in the following section), the mobilized strength ratio $\beta(m,n)$ after the excavation stage m for soil layer n can be found by reading off the stress-strain curve at the average shear strain level experienced by the nth layer in the mth stage of construction.

Shear Strength Mobilized within the Mechanism

In soft clay, the undrained shear strength generally varies with depth and with orientation of shear direction. The strength matrix $c_{\text{mob}}(m,n)$ mobilized for excavation stage m for layer n can be expressed using a matrix $\beta(m,n)$ on the appropriate undrained shear strength profile. Regarding orientation, anisotropy of soft soil can be a significant factor for excavation stability. For example, Clough and Hansen (1981) show an empirical factor on the basis of the observation that triaxial extension tests give roughly one-half the undrained shear strength of triaxial compression, with simple shear roughly halfway between. Fig. 4 shows the orientation of the major principal stress direction within the various zones of shearing in the assumed plastic mechanism for wide excavations and indicates with a code the soil-test configuration that would correctly represent the undrained shear strength of the specific orientation. For locations marked DSS, the assumed directions of shearing are either vertical or horizontal, so the ideal test on a vertical core is a direct simple shear test. In areas marked plane-strain active (PSA) and plain-strain passive (PSP), shearing takes place at 45° to the horizontal, and these zones are best represented by plane-strain active and passive tests, respectively. Since the undrained shear strength of the direct simple shear test is roughly the average of that of PSA and PSP, the relative influence of the PSA and PSP zones is roughly neutral with respect to direct simple shear. As a result, the design method for braced excavation can best be made on the basis of the undrained shear strength of a direct simple shear test. A similar decision was made by O'Rourke (1993).

The equilibrium of the unbalanced weight of soil inside the mechanism is achieved by mobilization of shear strength. For each excavation stage, the mobilization of shear strength for each layer is obtained by the following:

$$c_{u,\text{mob}}(m,n) = \beta(m,n)c_u(n) \tag{16}$$

in which $c_{u,\text{mob}}(m,n)$ = mobilized undrained shear strength for layer n after excavation stage m; $c_u(n)$ = undrained shear strength for layer n; and $\beta(m,n)$ = mobilized strength ratio for soil layer n after excavation stage m.

Incremental Energy Balance

By conservation of energy, the total loss of potential energy of the soil (ΔP) must balance the total work done in shearing the soil (ΔW) and the work done in bending the wall, which (in the absence of plastic yielding of the wall) will be the total elastic strain energy stored within it (ΔU):

$$\Delta P = \Delta W + \Delta U \tag{17}$$

The potential energy loss on the active side of the wall and the potential energy gain of soil on the passive side can be calculated easily. The net change of gravitational potential energy (ΔP) in the mth stage of construction is given by the sum of the potential energy changes in each layer:

$$\Delta P_m = \sum_{i=1}^{n}\left[\int_{\text{volume}} \gamma_{\text{sat}}(m,i)dw_y(m,i)d\text{Vol}\right] \tag{18}$$

in which $\delta w_y(m,i)$ = vertical component of displacement of soil in the ith layer for the mth stage of construction; $\gamma_{\text{sat}}(m,i)$ = saturated unit weight of soil in the ith layer for the mth construction. The total change in potential energy ΔP from the start of excavation is thus simply given by

$$\Delta P = \sum_{m=1}^{M} \Delta P_m \tag{19}$$

This procedure can obviously be simplified if all soil layers are of equal density.

Because there are no displacement discontinuities, the total work done in shearing the soil is given by summing for each layer:

$$\Delta W = \sum_{i=1}^{n}\left[\int_{\text{Volume}} \beta(m,i)c_u(m,i)|\delta\gamma(m,i)|d\text{Vol}\right] \tag{20}$$

in which $c_u(m,i)$ = undrained shear strength of soil in the ith layer for the mth stage of construction; $d\gamma(m,i)$ = shear strain increment of soil in the ith layer for the mth stage of construction; and the corresponding mobilized strength ratio is given by

$$\beta(m,i) = \frac{c_{u,\text{mob}}(m,i)}{c_u(m,i)} \tag{21}$$

The total elastic strain energy stored in the wall, ΔU, can be evaluated by repeatedly updating the deflected shape of the wall. It is necessary to do this since U is a quadratic function of displacement

$$\Delta U = \frac{EI}{2}\int_0^s \left[\frac{d^2 w_x}{dy^2}\right]^2 dx \tag{22}$$

in which E and I = the elastic modulus and the second moment of area per unit width of wall and s = length of the wall in bending, which is taken here to be the unsupported length of wall that can bulge below the lowest prop.

By assuming the cosine waveform equation [Eq. (1)], the strain energy term can be shown to be as follows:

$$\Delta U = \frac{\pi^3 EI\delta w_{\max}^2}{\lambda^3}\left[\frac{\pi s}{\lambda} + \frac{\sin(\frac{4\pi s}{\lambda})}{4}\right] \tag{23}$$

in which λ = wavelength of deformation and $dw_{\max}$ = maximum deflection of the wall in any given excavation increment.

Calculation Procedure

The following calculation procedure is programmed in Matlab version 2006b.

1. At each stage of excavation, a maximum deformation w_{max}, which is bounded by an upper and a lower bound, is assumed. The soil stratum is divided into n layers. The areas on both the active side and the passive side in each layer are calculated.
2. For each layer, the mobilized shear strain and the change in potential energy on both active and passive sides in different zones is calculated with the help of the numerical integration procedure in Matlab by using Eq. (18). The total mobilized shear strain is updated according to Eq. (15).
3. With the use of a suitable stress-strain curve (e.g., the simple shear stress-strain data shown in Fig. 7), the mobilized strength ratio β is found.
4. The total change in potential energy, the work done on the soil, and the elastic bending energy stored in the wall are calculated by Eqs. (19), (20), and (22), respectively.
5. By considering the conservation of energy of a structure in static equilibrium, the sum of work in the soil and stored energy in the wall must balance the total change in potential energy. To facilitate solving the solution, an error term is introduced as follows:

$$\text{Error} = \Delta W + \Delta U - \Delta P \tag{24}$$

6. When the error is smaller than a specified convergence limit, the assumed magnitude of deformation is accepted as the solution; otherwise, the method of bisection is employed to obtain another trial maximum displacement, and the error term is calculated again using steps 1–5.
7. The incremental wall movement profile is then plotted using the cosine function of Eq. (1).
8. The cumulative displacement profile is obtained by accumulating the incremental movement profiles.

Comparison with Numerical Analysis

The finite-element method can provide a framework for performing numerical simulations to validate the extended MSD method in evaluating the performance of braced excavations. However, finite-element analysis of retaining walls is potentially problematic. One the most challenging problems is choice of a constitutive model for the soil. A generalized stress-strain relationship can be very complicated when considering soil stress history and anisotropy (Whittle 1993).

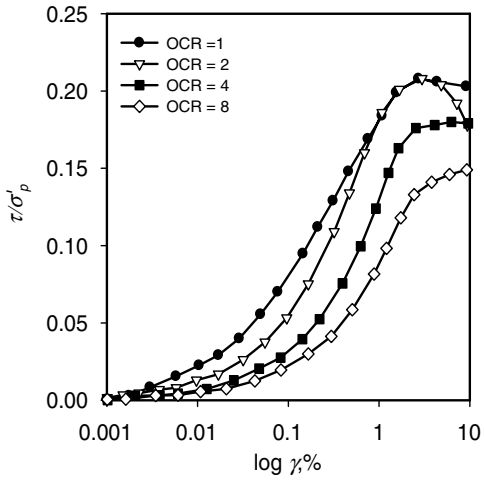

Fig. 7. Stress-strain response for K_o-consolidated undrained DSS tests on Boston blue clay (after Whittle 1993)

The validation of the extended MSD method is examined by comparing its predictions with results of comprehensive FE analyses of a plane-strain-braced excavation in Boston blue clay (BBC) carried out by Jen (1998). In these analyses, the MIT-E3 constitutive model is used (Whittle 1987) on the basis of Modified cam clay (Roscoe and Burland 1968). However, several modifications had been made to include small-strain nonlinearity, soil anisotropy, and the hysteretic behavior associated with reversal of load paths. Whittle (1993) also demonstrated the ability of the model to accurately represent the behavior of different clays when subjected to a variety of loading paths.

Example of MSD Calculation

The following example shows the extended MSD calculation of wall deflections for a 40-m deep wall retaining clay to a 17.5 m depth, creating an 80-m wide excavation with seven levels of support [Fig. 8(a)]. The construction sequence comprises the following steps:

1. The soil is excavated initially to an unsupported depth (h) of 2.5 m.
2. The first support is installed at the ground surface.
3. The next level of props is installed at a vertical spacing of 2.5 m, and 2.5 m of soil is excavated.
4. Step 3 is repeated up to an excavation depth of 17.5 m.

The undrained shear strength of the soil is expressed by the relationship suggested by Hashash and Whittle (1996) for Boston blue clay as follows:

$$c_u = 0.21[8.19z + 24.5] \text{ kPa} \tag{25}$$

The cantilever mode of deformation and the bulging movements are calculated separately using the mechanism of Osman and Bolton (2006) for Step 1 and the extended MSD method as described above for the succeeding steps. The total wall movements are then obtained by adding the bulging movements to the cantilever movement following Clough et al. (1989).

Cantilever Movement

By solving for horizontal force equilibrium and moment equilibrium at the top of the wall, the average mobilized shear stress (c_{mob}) is found to be 11.4 kPa. The mobilized strength ratio β is 0.29. The mobilized strain is then read off from the direct simple shear stress-strain data of Fig. 7, by using an appropriate preconsolidation pressure σ'_p and an appropriate OCR. The mobilized shear strain (γ_{mob}) is thereby found to be 0.2%. The corresponding wall rotation is therefore found to be 0.1%, giving a displacement of 39 mm at the top of the wall.

Bulging Movements

The first support is installed at the top of the wall. The length of the wall below the support is 40 m. By adopting an iterative calculation procedure and by using the deformation mechanism for a narrow excavation, the magnitude of bulging movement at each stage of excavation can be obtained. Then the incremental bulging movement profile in each stage is plotted by using the cosine function on the basis of the corresponding wavelength, which reduces as each level of props is placed. The total wall movement is obtained by superimposing the cantilever movement with all of the bulging movements for the successive stages of excavation. Fig. 8(a) shows the accumulated deformation profiles of the wall. In general, MSD predicted deeper maximum bulging displacements than the FEA of

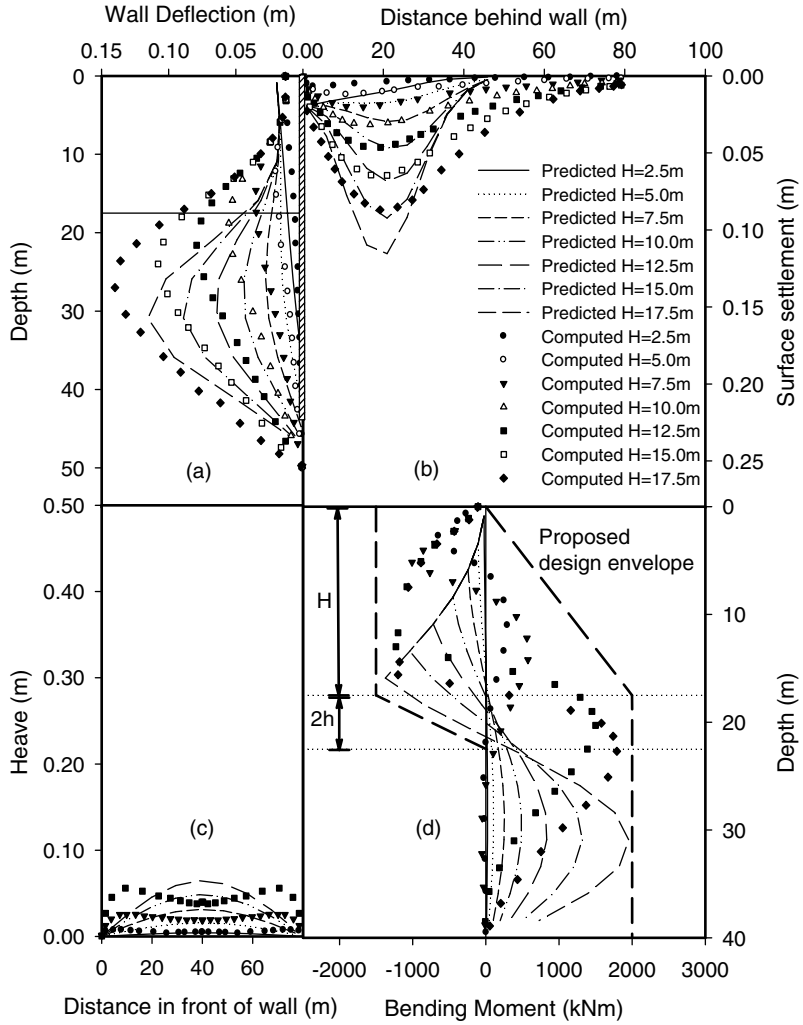

Fig. 8. Comparison of wall performance as predicted by MSD and as computed by FEA by Jen (1998; with permission from Massachusetts Institute of Technology)

Jen (1998). The maximum wall deflection predicted by MSD for an excavation depth of 17.5 m is 115 mm, which corresponds to 0.66% of the excavation depth. This underestimates the FEA by a factor of 1.2.

The final displacement profiles of ground settlement are obtained by summing up the incremental settlements in each stage of excavation and are given in Fig. 8(b). The maximum ground settlement predicted by MSD is 117 mm, which overpredicts the FEA by a factor of 1.3. Both the predicted and computed settlement troughs offer maximum settlements at 20 m (about 1.14 H) behind the diaphragm wall. The MSD prediction of base heave at different stages of excavation is compared with computed results in Fig. 8(c). The maximum base heave predicted by MSD is 64 mm, which overpredicts FEA by a factor of 1.1. To sum up, the maximum ground movements predicted by MSD fall within 30% of the FEA computation of Jen (1998).

Fig. 8(d) shows comparisons of the bending moments in the retaining wall obtained from FEA and those derived from MSD by using a simple finite-difference method. Despite the fact that the position of the MSD-predicted maximum bending moment occurs at a deeper level, the magnitude of the maximum bending moment compares very well with the computed result. A design envelope for bending moment is proposed on the basis of MSD predictions and accounting for the changes in profile as excavation proceeds. This gives the designer of a concrete diaphragm wall an apparently successful approximate criterion for the design of steel-reinforcement cages necessary for the prevention of plastic hinges.

The least successful aspect of the comparisons in Fig. 8 is the extent of the settlement trough on the retained soil surface. MSD strongly underestimates FEA settlement computations for separations $2H < x < 4H$. In offering a settlement trough of 50 m width, compared to about 80 m from FEA, MSD may be conservatively overpredicting ground curvatures in hogging, perhaps by a factor of up to 2. Such curvatures are used to assess the serviceability of existing structures or services adjacent to deep excavations. Apart from recognizing that MSD apparently errs on the safe side, we should recall that FEA generally predicts settlement troughs that are shallower and wider than those found in the field.

Database of Movements Caused by Deep Excavation in Soft Soil

The MSD procedure for estimating ground deformations in plane-strain caused by deep, undrained excavations is capable of accounting for factors such as ground stratification, soil nonlinearity, wall stiffness, and boundary conditions, which should be known at the design stage. Other factors, such as three-dimensional (3D) effects and the onset of consolidation and swelling, would require more

complete numerical analyses. And design uncertainties, such as the actual construction sequence in space and time and the workmanship involved in fixing struts, will only emerge during construction.

With the aim of gaining a better understanding of the predictability of actual ground deformations induced by deep excavations, a database of 155 international case histories was collected, each of which has been published in geotechnical journals, international conference proceedings, national technical reports, or dissertations. The main focus of these cases was on the deformation of walls supporting deep excavations in soft to firm clays (i.e., $c_u < 75$ kPa). For each case history, relevant information was extracted and analyzed, and major factors, such as soil properties, groundwater conditions, excavation geometry, stiffness of structural support system, construction method, and ground deformation responses, were considered. The details of each of these excavation case histories, together with the source references from which they were derived, can be found in Lam (2010).

Traditional Interpretation of Field Data

This section uses the new database to demonstrate the rather limited efficacy of current ways of presenting wall deformation data. In Fig. 9, the maximum horizontal wall displacement $w_{\max}$ is plotted against the excavation depth H with different icons used for different structural support systems. The values of maximum horizontal displacement scatter over a very wide range, showing that there is no simple linear relationship between horizontal wall displacement and excavation depth even for a specific wall type. For 55% of the cases, most of which are supported by diaphragm walls, the maximum displacement $w_{\max}$ is less than 0.5% H, whereas 26% of the cases show maximum displacements lying between 0.5% H and 1% H. Only in 19% of the cases, which always involve sheet piled excavations, are the maximum wall displacements greater than 1% H. Other plots are required to better understand the scatter.

Mana and Clough (1981) plotted the normalized maximum horizontal displacement $w_{\max}/H$ against a factor of safety against base heave (FOS) defined by Terzaghi (1943); this is shown for the new database in Fig. 10. Fig. 10 also shows the limits suggested by Mana and Clough for cases of excavation in soft soil supported by sheet pile walls. In general, the normalized horizontal displacement of walls from the new database decreases with increasing FOS as expected. Although the majority of the cases fall within the suggested limits, the measured wall movements for a typical FOS = 1.5 scatter between $w_{\max}/H = 0.2\%$ and 2.8%, demonstrating that there is no simple dependence of normalized wall movement with the FOS based on the soil strength alone. The traditional calculation of FOS does not account for governing factors such as soil stiffness and the structural stiffness of the support system.

Fig. 11 shows the normalized maximum horizontal wall displacement versus the system stiffness (η) as defined by Clough et al. (1989):

$$\eta = \frac{EI}{\lambda_w h^4} \tag{26}$$

in which EI = flexural stiffness of the wall, h = representative vertical spacing between supports, and γ_w = unit weight of water. Again, the field data scatter over a wide range, although the general trends of a decrease in displacement with increasing system stiffness and soil FOS are those suggested by Clough et al. (1989). Nevertheless, a calculated safety factor of about 1 could lead to an observed maximum wall displacement $w_{\max}/H$ as low as 0.1%, though the value expected by Clough et al. was about 1% for even the stiffest support system. Similar observations were made with other databases by Moorman (2004) and Long (2001).

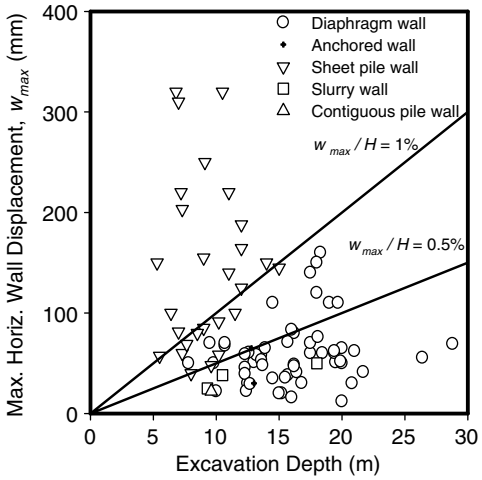

Fig. 9. Normalized horizontal wall displacement with different support systems

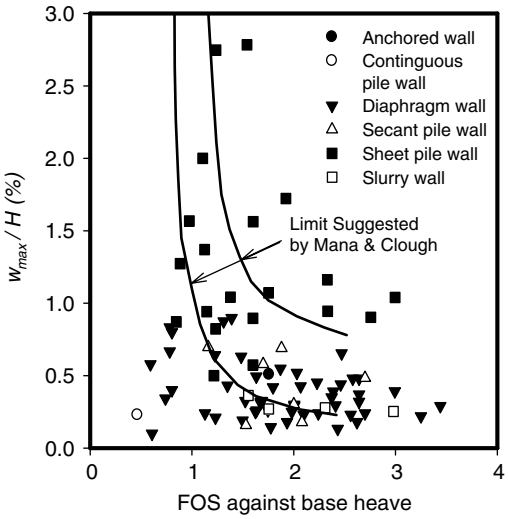

Fig. 10. Variation of normalized horizontal wall displacement (adapted from Mana and Clough 1981, ASCE)

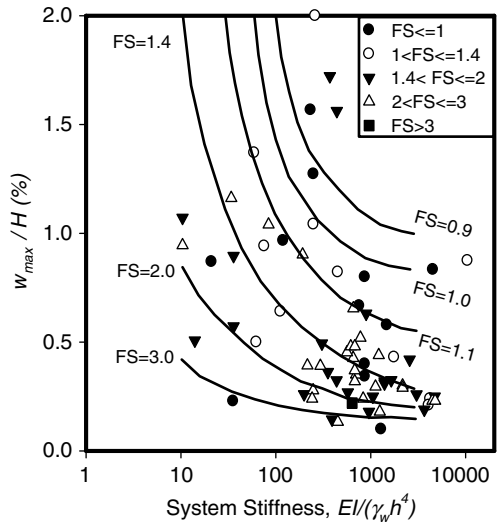

Fig. 11. Variation of maximum horizontal wall displacement with system stiffness and factor of safety against base heave, following Clough et al. (1989, ASCE)

Apparently, the factor of safety against base heave is not an ideal measure to quantify ground movements caused by deep excavation even when the wall stiffness is accounted for. Soil stiffness is also a significant parameter, as subsequently described.

Performance of MSD Method in Estimating Deformations around Deep Excavations

A total of 110 out of 155 case histories, from nine cities worldwide, were fully documented so that an analysis could be conducted with the incremental form of the MSD method, taking careful consideration of ground stratification, system stiffness and prop spacing, and excavation geometry, including excavation depth and breadth, depth to stiff layer, undrained shear strength profile, and soil stiffness.

Fig. 12 shows the degree of mobilization β of shear strength versus strain in tests reported for the nine soils concerned. The excavation case-specific information from the database was used directly in MSD to predict maximum wall displacements for each stage of excavation, which are compared with writers' reported observations in Fig. 13. Results show a correlation coefficient $R^2 = 0.83$ around the line 1:1 with a coefficient of variation of 0.24. More than 90% of the MSD predictions, typically for each

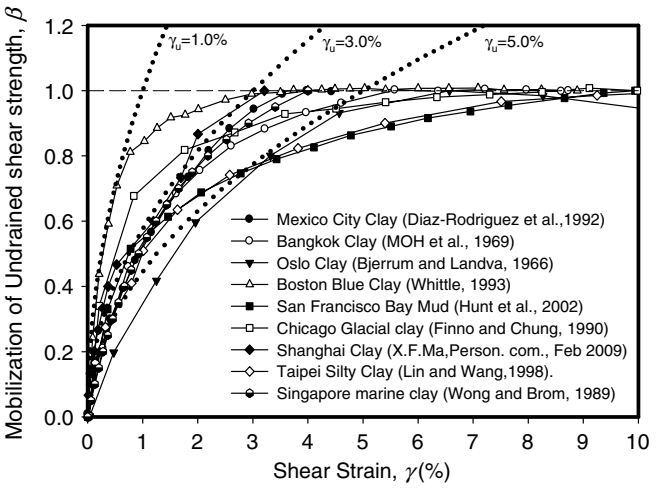

Fig. 12. Stress-strain relationship of soft clays worldwide

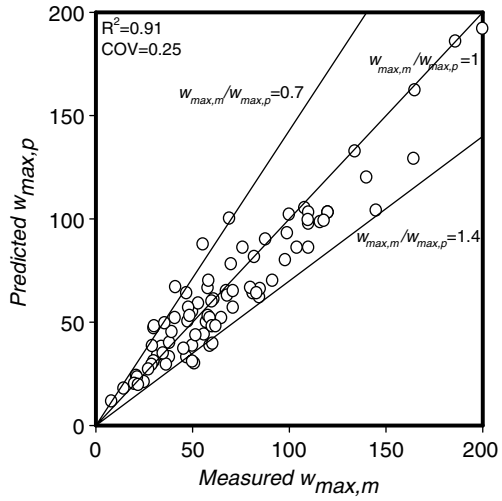

Fig. 13. Comparing measured lateral wall displacements with MSD predictions

of four excavation levels, fell within 30% of the corresponding observations. Considering the lack of any detailed account of soil anisotropy, the field performance of MSD is evidently quite satisfactory.

Simplified Relationship between Wall Deflections and Mobilization of Soil Strength

Following the logic of MSD, a simplified but sound way of analyzing data from the whole database can now be introduced. According to the requirement of soil-structure compatibility and the kinematics of mechanisms involved in deep excavations as shown in Fig. 3, the wall deflection $w_{\max}$ can be related to the average shear strain γ_{ave} in the adjacent soil mass by the following:

$$w_{\max} \approx \lambda \gamma_{ave}/2 \tag{27}$$

in which λ = typical wavelength that defines the size of the zone of deformation. For the field case studies, which were all on excavations with fixed-based walls, the wavelength is always limited by the depth of the soft clay stratum. In other words, it is defined at any stage as the distance between the lowest prop level and the base of the clay stratum. Because of the incremental nature of a multiprop excavation, the average wavelength can be taken as

$$\lambda_{ave} \approx C - (H - h)/2 \tag{28}$$

in which C and H = depth of clay stratum and ultimate excavation depth, respectively, and h = vertical prop spacing.

The second element of MSD is to relate the shear strain to the mobilization of soil strength by considering the shear stress-strain properties of representative soils. A mobilization factor was defined in the UK Code of Practice on Earth Retaining Structures (BS 8002 1994) as follows:

$$M = \frac{c_u}{c_{\text{mob}}} = \frac{1}{\beta} \tag{29}$$

The degree of strength mobilization is controlled by shear strain through the stress-strain relation.

Shearing within the retained soil mass is characterized by principal stress rotation and is best approximated by data from direct simple shear tests. The use of undrained direct simple shear tests is well developed for geotechnical engineering design in soft ground construction (e.g., Ladd and Foott 1974). Fig. 12 summarizes the mobilized shear strength ratio (β) obtained mainly from undrained direct simple shear (DSS) tests on a variety of soft clays worldwide. For $\beta < 0.8$, these clays are well described by a parabolic relation:

$$\frac{\gamma}{\gamma_u} = \left(\frac{c_{\text{mob}}}{c_u}\right)^2 = \left(\frac{1}{M}\right)^2 \quad \text{for } \beta < 0.8, \text{ i.e., } M \geq 1.25 \tag{30}$$

in which γ_u = reference strain obtained by extrapolating approximately parabolic small-strain data to intersect the peak strength asymptote. These curves, superimposed on the data in Fig. 12, tend to fall within a range of γ_u from 1% to 5%. For very soft and high plasticity clays like Oslo clay, the reference strain value can be larger than 5%, whereas the shear strength of firm and low-plasticity Boston blue clay is mobilized at a smaller reference strain of about 1%. When the reference strain is used to normalize the small-strain power-law stiffness of soil, a simple relation can be obtained from Eqs. (27)–(30) to define a normalized displacement factor ψ for deep excavations as follows:

$$\psi = \frac{2w_{\max}}{\lambda_{ave}\gamma_u} = \frac{2w_{\max}}{[C-(H-h)/2]\gamma_u} \tag{31}$$

The approximate parabolic fitting, for $\beta \le 0.8$ ($M \ge 1.25$) in Fig. 12 permits a further prediction:

$$\psi = \left(\frac{1}{M}\right)^2 \quad \text{for } \beta < 0.8, \text{ i.e., } M \ge 1.25 \tag{32}$$

The records of field displacements from the database permit the direct calculation of displacement factor ψ from Eq. (31), where the characteristic shear strain γ_u is known. We might expect that ψ will vary between 0 and 1 and that it will decrease as the stiffness of the support system increases. The newly extended MSD theory enables a prediction to be made of the variation of ψ with the system stiffness ($\eta = EI/\gamma_w h^4$) as defined by Eq. (26). An MSD chart of ψ versus η, for various values of the ratio (H/C) of excavation depth to the depth of fixity in the stiff layer, calculated for a typical soft clay strength profile and a stress-strain curve with $\gamma_u = 3\%$, is given in Fig. 14(a). Although the present analysis does not consider other factors such as consolidation effects, corner effects, and workmanship, the MSD trend lines are broadly consistent with the field data. However, it should be noted that when the parabolic stress-strain approximation leads to calculated values of ψ in excess of 0.64, the field measurements can significantly exceed the MSD prediction [see the square icons lying above the uppermost MSD prediction in Fig. 14(a)]. Fig. 14(b) repeats the MSD prediction of ψ versus η, but for selected values of $\gamma_u = 1\%$, 3% and 5% for the particular excavation geometry. γ_u is embodied in the definition of ψ itself, through Eq. (31). Accordingly, although γ_u is found in Fig. 14 not to influence very strongly the predicted displacement factor ψ, at least for flexible walls ($\eta \le 10^2$), the predicted wall displacement remains proportional to γ_u through Eq. (31).

As mentioned previously, a warning is included in Fig. 14 against using the simple parabolic prediction of displacement factor ψ in the case of $\psi_{MSD} > 0.64$, corresponding to $M < 1.25$ or $\beta > 0.8$. For these very large mobilizations of strength, the strains measured in the soil tests, reported in Fig. 12, invariably exceeded the parabolic fitting to small-strain data. So Eq. (32) will probably underestimate field deformations. For a typical excavation in typical soft clay with $\gamma_u = 3\%$, the limitation $\psi_{MSD} = 0.64$ corresponds to limiting $w_{\max}/H \approx 1\%$, which would already be excessive if there were any structures or services within the zone of influence. Furthermore, the adoption of a mobilization factor (or factor of safety) below 1.25 would often be considered unwise, especially considering the possibility of adhesion on the retaining wall being smaller that the soil strength c_u and of its dropping further as a result of soil sensitivity. Even this degree of caution leaves the engineer free to accept a greater wall deformation of $w_{\max}/H \approx 1.5\%$ in more compliant soils ($\gamma_u \approx 5\%$). The rational selection of a mobilization/safety factor with respect to separate safety and displacement criteria is a particular opportunity afforded by the MSD approach.

If an engineer wants to design a structure to support an excavation with a specified excavation geometry in soil with a stress-strain curve that can be estimated and if the permissible wall deflection is specified, the equivalent normalized displacement factor ψ can be deduced. The required system stiffness can then be read off from the trend lines in Fig. 14(b). For instance, to design a 20-m deep excavation in a 30-m-thick very soft soil with a reference strain γ_u of 3% and a maximum permissible lateral wall movement of 100 mm, simple calculations [Eq. (31)] tell the engineer that the displacement factor ψ should be about 0.33. From the design trend line, a support system with a system stiffness η of about 1,170 is recommended; this could correspond to a 0.8-m-thick diaphragm wall with a support spacing of about 3 m (giving $\eta \approx 1,230$).

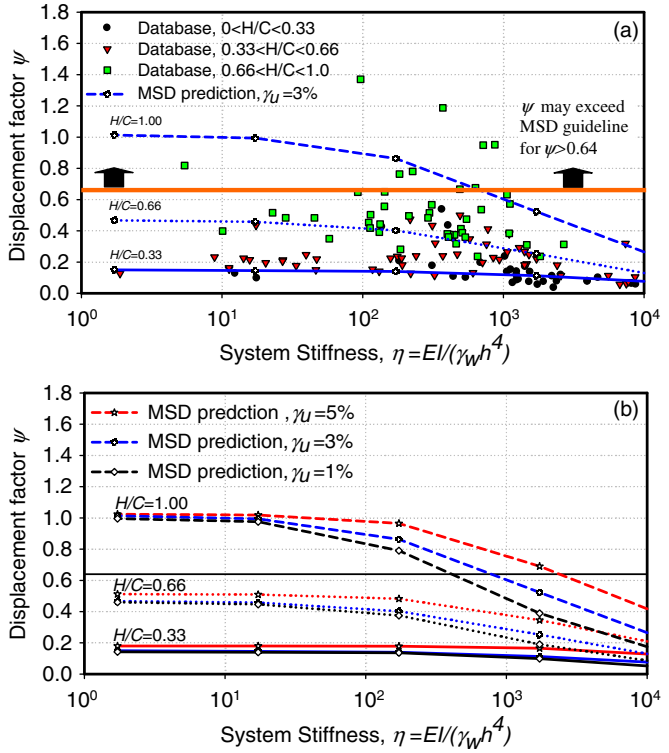

Fig. 14. Variation of displacement factor ψ with system stiffness defined by Clough (1989): (a) data and MSD prediction for $\gamma_u = 3\%$; (b) MSD prediction for $\gamma_u = 1\%$, 3%, and 5%

Although this simplified approach can apparently provide approximate but reasonably robust answers to key design questions and do so simply by inspection of a chart, there is no particular justification for the use of system stiffness parameter η beyond that originally given by Clough et al. (1989). Further refinement of the different influences of prop spacing and wall flexural stiffness should ultimately be possible. Nevertheless, the opportunity to include strain to failure γ_u in simple wall movement predictions should lead engineers to consider soil stiffness as a key factor in the design of deep excavations and to request stress-strain data accordingly.

Conclusions

This paper introduces an improved MSD method to calculate the displacement profile of a multipropped wall retaining an excavation in soft clay, which is taken to involve undrained soil behavior during construction. As with the earlier MSD approach, each increment of wall bulging, generated by excavation of soil beneath the current lowest level of support, is approximated by a cosine function. The soil is divided into layers in which the average shear strain increments are compounded so that the mobilized strength ratio in each layer can be tracked separately as excavation proceeds by using normalized stress-strain data from DSS tests matched to the soil properties at the middepth of each layer. The incremental loss in potential energy associated with the formation of a settlement trough, a result of wall deformation and base heave, can be expressed as a function of those ground movements at any stage. By conservation of energy, this must always balance the sum of

incremental work done in shearing the soil and the incremental storage of elastic strain energy in bending the wall. By using an iterative procedure, the developing profile of wall displacements can be found.

A reasonable agreement is found between predictions made of wall displacements, ground settlements, base heave, and bending moments by using this extended MSD method and the FEA results of Jen (1998), who created full numerical solutions by using the MIT-E3 soil model. Although there were some discrepancies in the precise location of the point of maximum bulges, the shape of the wall profile was broadly correct, and the magnitude of the maximum displacement was 20% underpredicted by MSD compared with the FEA values. The magnitude of maximum settlement was 30% overpredicted by MSD compared with FEA, which also gave a characteristically wider settlement trough. Maximum wall bending moments produced by MSD corresponded quite closely to FEA computations, although the computed location of the maximum value was significantly higher. Nevertheless, it is proposed that a relatively straightforward MSD analysis, which could be performed within an hour or two by a design engineer, could be a useful tool in making key design decisions, even if it serves as a precursor to more elaborate FEA.

In order to assess the capability of MSD to produce useful wall displacement predictions in actual field conditions, a new database has been created of 155 case histories of walls that could be taken to be fixed in a hard layer at their toe but otherwise were retaining soft to firm clays. This is a much larger database than has previously been collected. It was shown for 110 well-documented field studies that incremental MSD analyses were capable of making predictions of maximum wall movement in 90% of these cases within 30% of the actual field values.

Since MSD is semianalytical, it could also be used to generate a more rational normalization of maximum excavation-induced wall displacement, by using the parameter $\psi = 2w_{max}/[C-(H-h)/2]\gamma_u$. This normalization recognizes that if all details of excavation geometry, wall stiffness, and support remain the same, w_{max} should be proportional to the size of the ground deformation mechanism induced by the various stages of excavation and also proportional to the characteristic soil strain γ_u defined by the intersection of the small-strain nonlinear stress-strain curve extended to meet the peak strength asymptote. This newly defined characteristic soil shear strain γ_u is a promising index parameter that might be taken to lie between 1% for firm, low-plasticity clays and 5% for soft, high-plasticity clays. Further work offering statistical correlations for γ_u in terms of basic soil properties would be useful.

A new chart of ψ versus normalized system stiffness $\eta = EI/\gamma_w h^4$ was used to demonstrate that MSD could correctly capture the trend of wall displacements increasing with the ratio (H/C) of excavation depth to the depth of fixity in the stiff base layer. Further work needs to be done to refine the separate effects of ψ reducing with reduced prop spacing h and with increased wall stiffness EI.

Acknowledgments

The writers would like to acknowledge the Platform Grant (GR/T18660/01) awarded by the UK Engineering and Physical Sciences Research Council. We were alerted to the extensive field records of excavations in Shanghai through a presentation by Dr. Xu of Eastern China Architectural Design and Research Institute (ECADI) at an Engineering and Physical Science Research Council (EPSRC) UK–China GEONET meeting in Ningbo in September 2008. We are grateful to Dr. Xianfeng Ma for help in translating key terms in Dr. Xu's Ph.D. thesis.

Notation

The following symbols are used in this paper:

A = area of deformation mechanism;
B = breadth of excavation;
C = depth of soft soil stratum;
c_u = undrained shear strength;
$c_{u,mob}$ = mobilized undrained shear strength;
E_t = tangential elastic modulus;
EI = bending stiffness of retaining wall;
FOS = factor of safety against base heave;
H = excavation depth;
h = prop spacing;
K = system stiffness;
L = length of retaining wall;
OCR = overconsolidation ratio;
t = wall thickness;
s = unsupported length of the wall;
w = gravimetric water content;
w_{max} = maximum later wall displacement;
z = depth below ground surface.
β = mobilized strength ratio;
γ = total shear strain;
λ = wavelength of deformation;
γ_{ave} = average mobilized shear strain;
γ_{mob} = mobilized shear strain;
γ_{sat} = saturated unit weight;
γ_u = reference strain;
ΔD = energy dissipation as a result of plastic shearing;
ΔP = loss of potential energy;
ΔU = elastic strain energy;
δw = incremental lateral wall displacement;
δw_{max} = maximum incremental lateral wall displacement;
$\delta\gamma$ = incremental shear strain;
ε_1 = major principle strain;
σ_1 = major principle stress;
σ_3 = minor principle stress; and
σ'_p = preconsolidation pressure.

References

Bjerrum, L., and Eide, O. (1956). "Stability of strutted excavations in clay." *Geotechnique*, 6, 115–128.

Bolton, M. D., Lam, S. Y., and Osman, A. S. (2009). "Geotechnical aspects of underground construction in soft ground." *Proc., 6th Int. Symp.*, CRC Press, London, 15–28.

Bolton, M. D., and Powrie, W. (1987). "Behaviour of diaphragm walls retaining walls prior to collapse." *Geotechnique*, 37(3), 335–353.

Bolton, M. D., Powrie, W., and Symons, I. F. (1989). "The design of stiff in-situ walls retaining overconsolidated clay part." *Ground Eng.*, 22(8), 44–48.

Bolton, M. D., Powrie, W., and Symons, I. F. (1990a). "The design of stiff in-situ walls retaining over-consolidated clay. Part 1: Short term behaviour." *Ground Eng.*, 22(9), 34–39.

Bolton, M. D., Powrie, W., and Symons, I. F. (1990b). "The design of stiff in-situ walls retaining over-consolidated clay. Part II: Long term behaviour." *Ground Eng.*, 23(2), 22–28.

BSI 8002. (1994). "Code of practice for earth retaining structures." British Standards Institution, London.

Clough, G. W., and Hansen, L. A. (1981). "Clay anisotropy and braced wall behavior." *J. Geotech. Eng.*, 107(7), 893–913.

Clough, G. W., Smith, E. W., and Sweeney, B. P. (1989). "Movement control of excavation support system by iterative design." *Foundation engineering current principles and practices*, ASCE, New York, 2, 869–882.
Eide, O., Aas, G., and Josang, T. (1972). "Special application of cast-in-place walls for tunnels in soft clay." *Proc., 5th European Conf. on Soil Mechanics and Foundation Engineering*, Madrid, Spain, 1, 485–498.
Hashash, Y. M. A., and Whittle, A. J. (1996). "Ground movement prediction for deep excavations in soft clay." *J. Geotech. Eng.*, 122(6), 474–486.
Jen, L. C. (1998). "The design and performance of deep excavations in clay." Ph.D. thesis, Dept. of Civil and Environmental Engineering, Massachusetts Inst. of Technology, Cambridge, MA.
Klar, A., and Osman, A. S. (2008). "Load-displacement solutions for pile and shallow foundations abased on deformation fields and energy conservation." *Geotechnique*, 58(7), 581–589.
Ladd, C. C., and Foott, R. (1974). "New design procedure for stability of soft clays." *J. Geotech. Engrg. Div.*, 100(GT7), 763–786.
Lam, S. Y. (2010). "Ground movements due to excavation in clay: physical and analytical models." Ph.D. thesis, Cambridge Univ., Cambridge, UK.
Long, M. (2001). "Database for retaining wall and ground movements due to deep excavations." *J. Geotech. Geoenviron. Eng.*, 127(3), March, 2001, 203–224.
Mana, A. I., and Clough, G. W. (1981). "Prediction of movements for braced cut in clay." *J. Geotech. Engrg. Div.*, 107(6), 759–777.
Milligan, G. W. E., and Bransby, P. L. (1976). "Combined active and passive rotational failure of a retaining wall in sand." *Geotechnique*, 26(3), 473–494.
Moormann, C. (2004). "Analysis of wall and ground movements due to deep excavations in soft soil based on a new worldwide database." *Soils Found.*, 44(1), 87–98.
O'Rourke, T. D. (1993). "Base stability and ground movement prediction for excavations in soft clay." *Retaining structures*, Thomas Telford, London, 131–139.
Osman, A. S., and Bolton, M. D. (2004). "A new design method for retaining walls in clay." *Can. Geotech. J.*, 41(3), 451–466.
Osman, A. S., and Bolton, M. D. (2005). "Simple plasticity-based prediction of the undrained settlement of shallow circular foundations on clay." *Geotechnique*, 55(6), 435–447.
Osman, A. S., and Bolton, M. D. (2006). "Ground movement predictions for braced excavations in undrained clay." *J. Geotech. Geoenviron. Eng.*, 132(4), 465–477.
Osman, A. S., Bolton, M. D., and Mair, R. J. (2006). "Predicting 2D ground movements around tunnels in undrained clay." *Geotechnique*, 56(9), 597–604.
Roscoe, K. H., and Burland, J. B. (1968). "On the generalized stress-strain behaviour of 'wet' clay." *Engineering plasticity*, J. Heyman and F. A. Leckie, eds., Cambridge University Press, Cambridge, UK.
Skempton, A. W. (1951). "The bearing capacity of clays." *Proc., Building Research Congress*, London, 180–189.
Sloan, S. W. (1988). "Lower bound limit analysis using finite elements and linear programming." *Int. J. Numer. Anal. Methods Geomech.*, 12(1), 61–77.
Sloan, S. W., and Kleeman, P. W. (1995). "Upper bound limit analysis using discontinuous velocity fields." *Comput. Methods Appl. Mech. Eng.*, 127, 293–314.
Terzaghi, K. (1943). *Theoretical soil mechanics*, Wiley, New York.
Ukritchon, B., Whittle, A. J., and Sloan, S. W.(2003). "Undrained stability of braced excavations in clay." *J. Geotech. Geoenviron. Eng.*, 129(8), 738–755.
Whittle, A. J. (1987). "A constitutive model for overconsolidated clays with application to the cyclic loading of friction piles." Ph.D. thesis, Dept. of Civil and Environmental Engineering, Massachusetts Inst. of Technology, Cambridge, MA.
Whittle, A. J. (1993). "Evaluation of a constitutive model for overconsolidated clays." *Geotechnique*, 43(2), 289–313.